American Mineralogist, Volume 104, pages 588–594, 2019

Phase transition of wadsleyite-ringwoodite in the Mg_2SiO_4-Fe_2SiO_4 system

Noriyoshi Tsujino[1,*], Takashi Yoshino[1], Daisuke Yamazaki[1], Moe Sakurai[1,2], Wei Sun[1], Fang Xu[1], Yoshinori Tange[3], and Yuji Higo[3]

[1]Institute for Planetary Materials, Okayama University, 827 Yamada, Misasa, Tottori 682-0193, Japan
[2]Department of Earth and Planetary Sciences, Tokyo Institute of Technology, 2-12-1 Ookayama, Meguro, Tokyo 152-8551, Japan
[3]Japan Synchrotron Radiation Research Institute, 1-1-1 Kouto, Sayo, Hyogo 689-5198, Japan

Abstract

The Fe-bearing wadsleyite-ringwoodite phase transition loop under dry conditions in a temperature range of 1473 and 1873 K was determined by in situ X-ray diffraction experiments at the synchrotron facility SPring-8. Pressure at high temperature was precisely determined within a 0.23 GPa error using in situ X-ray diffraction of MgO as a pressure standard. Under dry conditions, assuming an equilibrium chemical composition of wadsleyite and ringwoodite coexisting with garnet in a pyrolite model and an adiabatic temperature gradient with a potential temperature of 1550–1650 K, the phase transition depth and effective width of the seismic discontinuity were found to be 500–514 and 20–22 km, respectively. This effective width, which is three times greater than that of the olivine-wadsleyite phase boundary, can reflect a seismic wave of approximately 0.25 Hz. The wider transition loop between wadsleyite and ringwoodite could create a broad seismic discontinuity. Considering wet and oxidized conditions, the depth of the wadsleyite-ringwoodite phase boundary could be greater than 520 km assuming the small temperature dependency on water and oxygen fugacity effects. Variation in the depth of seismic anomaly may be attributed to water content or oxygen fugacity of the transition zone.

Keywords: Mantle, wadsleyite, ringwoodite, phase boundary loop, in-situ experiments

Introduction

Various seismic discontinuities in the Earth's interior have been globally determined by various seismic studies (e.g., Dziewonski and Anderson 1981). Phase transitions in the major constituent minerals are believed to cause such global discontinuities in the Earth's mantle. According to the velocity model (IASP91) proposed by Kennett and Engdahl (1991), an increase in P- and S-wave velocities by 3.6 and 4.1%, respectively, can be explained by the olivine-wadsleyite phase transition at 410 km seismic discontinuity. The post-spinel phase transition accounts for the 660 km seismic discontinuity characterized by P- and S-wave velocity increases of 5.8 and 6.3%, respectively. However, the phase transition between wadsleyite and ringwoodite produces velocity increases of only 1% or less (Helffrich 2000). Although several seismic studies using long period seismograms have suggested that the 520 km seismic discontinuity is a global feature (e.g., Shearer 1990, 1991; Flanagan and Shearer 1998), recent seismic studies demonstrated that this discontinuity is not a ubiquitous feature and is lacking in some regions (Gossler and Kind 1996; Deuss and Woodhouse 2001). In some cases, two discontinuities at approximately 500 and/or 560 km depths were detected rather than the 520 km seismic discontinuity (Deuss and Woodhouse 2001). Therefore, to understand the nature of the 520 km seismic discontinuity, it is important to accurately determine the phase boundary between wadsleyite and ringwoodite as a function of temperature, pressure, and chemical composition.

Temperature is among the key parameters that constrain the structure and composition of the Earth's interior. Although geophysical observations allow for the precise determination of depth, and hence, pressure, it is difficult to determine the temperature at a given depth without knowledge of mineral physics. The combined studies of potential temperature (e.g., McKenzie and Bickle 1988), phase boundary depth of constituent minerals, and depth of seismic discontinuities (Akaogi et al. 1989; Katsura et al. 2004) have made it possible to estimate a temperature profile of the Earth's mantle. The phase boundary binary loop between wadsleyite and ringwoodite is among the most important interfaces of the major predicted phase transitions used to constrain the mantle geotherm.

Using in situ X-ray diffraction at a synchrotron facility, Morishima et al. (1994) and Katsura et al. (2004) determined the olivine-wadsleyite phase boundary in the Mg-end-member and Fe-bearing systems, respectively. The phase boundary between wadsleyite and ringwoodite has only been determined in the Mg-end-member system by in situ studies (Inoue et al. 2006; Suzuki et al. 2000), while the phase boundary loop of wadsleyite-ringwoodite in Fe-bearing systems has only been estimated through thermodynamic calculations (Akaogi et al. 1989; Frost 2003) and quench experiments (e.g., Katsura and Ito 1989). In this study, we determined the precise pressure of the phase boundary loop between wadsleyite and ringwoodite at various temperatures under dry conditions via in situ high-pressure experiments. We also discuss the origin of the 520 km seismic discontinuity based on the wadsleyite-ringwoodite phase transition.

Experimental methods

In situ X-ray diffraction experiments were conducted using a Kawai-type multi-anvil apparatus SPEED-1500 installed at the beamline BL04B1 of the synchrotron facility SPring-8 (Utsumi et al. 1998). The pressure medium was an

* E-mail: tsujino@okayama-u.ac.jp

0003-004X/19/0004–588$05.00/DOI: https://doi.org/10.2138/am-2019-6823

octahedron composed of 5 wt% Cr_2O_3-doped MgO with an edge length of 10 mm. The pressure medium was compressed using tungsten-carbide anvils with 4 or 5 mm truncated edge lengths. Olivine with a composition of $(Mg_x,Fe_{1-x})_2SiO_4$, where x = 0.97, 0.91, 0.80, and 0.70, was used as a starting material. For x = 0.91, natural olivine from San Carlos, Arizona, U.S.A. was used. Other olivine compositions were synthesized using oxide powders, which were also used by Katsura et al. (2004). A powder mixture composed of MgO with 10 wt% Pt, or 20 wt% h-BN only for S3323, to suppress grain growth, was used as a pressure marker. Figure 1 shows the design of the cell assembly for the in situ X-ray diffraction experiments at high pressures and temperatures. Two samples with different Fe contents and a pressure marker, separated by Mo foils (30 μm), were packed into a graphite capsule. Oxygen fugacity was controlled to be similar to the Mo-MoO_2 buffer, which is near to that of the Fe-FeO buffer, using a Mo foil inside the graphite capsule. The thickness of each sample and the pressure marker was ~300 μm. A cylindrical TiB_2 + BN + AlN composite (with 2.6 and 2.0 mm outer and inner diameter, respectively, and 6.3 mm in length) was used as a heater. Cylindrical $LaCrO_3$ was used as a thermal insulator surrounding the heater. The temperature difference between the center and edge of the capsule was estimated to be approximately 50 K by the compositional difference [Mg# = Mg/(Mg+Fe) × 100] of the wadsleyite and ringwoodite of S3255 and 5K3134, assuming that the pressure was constant in the graphite capsule. Therefore, the maximum temperature difference was less than 50 K around the cylindrical X-ray window composed of the MgO placed in the thermal insulator. The temperature was monitored by a W3%Re-W25%Re thermocouple, whose junction was sandwiched between the MgO disks 0.2 mm in thickness adjacent to the pressure marker, to minimize the temperature difference between the thermocouple junction and the pressure marker, for a precise pressure calculation using the equation of state of MgO. The maximum temperature difference estimated at the pressure marker position was 25 K, corresponding to a pressure difference of 0.16 GPa when we used the equation of the state of MgO proposed by Tange et al. (2009).

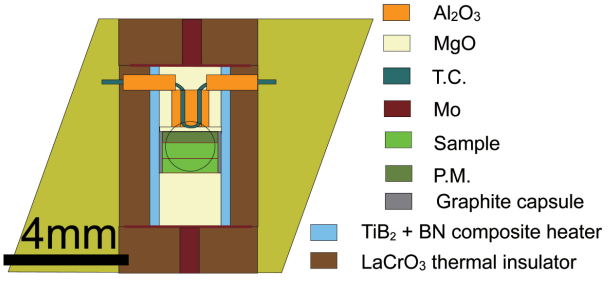

Figure 1. Schematic illustration of the cell assembly for the in situ X-ray diffraction experiments. (Color online.)

A solid-state detector connected to a multi-channel analyzer was used to collect the X-ray diffraction data. The energy was calibrated with the characteristic X-rays of Pb, Au, Pt, Ta, Ag, Mo, and Cu or the γ-ray of ^{55}Fe, ^{57}Co, and ^{133}Ba. The diffracted X-rays from the sample and pressure marker were collected at a fixed 2θ angle of 6° using the energy-dispersive method. The 2θ angle was calibrated using the MgO unit-cell volume in the pressure marker calculated by the (111), (200), (220), (311), and (222) diffraction peaks at ambient conditions except for Run No. S3323. During run no. S3323, the (111), (220), (311), (222), and (400) diffraction peaks of MgO were used to calibrate the 2θ angle because the (200) diffraction peak overlapped with that of cubic-BN at a high pressure and temperature. Errors in the pressure calculation were recorded as deviations in the individual peak positions, which were a maximum of 0.23 GPa and an average of 0.16 GPa. The sample was compressed to a desired pressure and then heated to a desired temperature (see Table 1). To establish the chemical equilibrium between wadsleyite and ringwoodite, the desired temperature was maintained for 1 to 8 h (see Table 1). Generally, after the desired temperature is reached, the pressure slightly decreases (e.g., Nishiyama et al. 2004). To confirm the chemical equilibrium in the samples after settling the pressure by a different pressure-temperature path, in S3323 the pressure was maintained at a higher level than that immediately after the desired temperature was reached by additional compression. The X-ray diffraction data were collected from the pressure marker immediately before quenching, to determine the precise pressure at high temperatures. The pressure was determined using the third-order Birch-Murnaghan equation of state (3BM) of MgO proposed by Tange et al. (2009) and Speziale et al. (2001).

To confirm the chemical equilibrium between wadsleyite and ringwoodite, additional quench experiments using the same cell assembly as the in situ experiments were conducted at ~14 GPa and 1673 K for 1 h. Two samples were set in the same run; one being an olivine powder with a composition of x = 0.80 that was the same as that used in in-situ experiments, and the other a mixture of olivine powder of x = 0.97 and 0.70 with a bulk composition of x = 0.80. At a high pressure and temperature, wadsleyite and ringwoodite were formed by the decomposition of the olivine powder with x = 0.80, while these were formed by the reverse reaction from the mixture of olivine powder with x = 0.97 and x = 0.70.

After the annealing experiments, the recovered samples were mounted in an epoxy resin and polished with diamond paste (1 μm in grain size). The chemical compositions of the coexisting wadsleyite and ringwoodite were measured using an electron probe micro-analyzer. (EPMA, JEOL-8800) combined with wavelength-dispersion spectroscopy (WDS) at the Institute for Planetary Materials, Okayama University. An accelerating voltage and a beam current of 15 kV and 1.2×10^{-8} A, respectively, were applied at an interval of 20 s for the peak and 10 s for the background signals. For each phase in recovered samples, typically 5 or more chemical compositional measurements were conducted at various positions. The standards for quantitative analyses of the sample composition were periclase, hematite, and wollastonite for MgO, FeO, and SiO_2, respectively. All the measurements were validated with reference to olivine.

Table 1. Result of in situ annealing experiments

Run no.	Load (ton)	TEL (mm)	*T* (K)	Duration (h)	Wd (Mg#)	Rw (Mg#)	K_D[c]	MgO V/V_0	*P* (GPa)	
									Tange (3BM)	Speziale
S2932	350	5	1473	7	81.1(3)	68.4(7)	0.51(1)	0.96874(65)	12.62(15)	12.94(13)
S2840	450	4	1473	3	87.2(3)	77.8(5)	0.52(1)	0.96007(22)	14.28(5)	14.46(4)
S2947	580	5	1473	3	93.2(2)	88.3(3)	0.55(2)	0.95301(90)	15.68(23)	15.88(19)
S3323[d]	650 to >720	5	1673	8	83.2(2)	75.5(3)	0.62(1)	0.96684(53)	14.27(12)	14.47(10)
S3254	800	5	1673	6	85.1(3)	78.1(1)	0.63(1)	0.96462(57)	14.69(13)	14.90(11)
S2910	600	5	1673	2	85.3(6)	77.2(6)	0.58(3)	0.96311(56)	14.98(13)	15.19(11)
S2823	500	4	1673	1	85.5(4)	77.6(3)	0.58(1)	0.96310(88)	15.13(21)	15.20(17)
S2917	700	5	1673	2	92.9(3)	88.4(3)	0.58(2)	0.95559(89)	16.46(23)	16.75(16)
S2838	500	4	1873	1	75.1(5)	65.5(7)	0.63(2)	0.97802(79)	13.52(16)	13.89(14)
S2893	560	5	1873	1	80.6(3)	71.3(2)	0.60(1)	0.97194(85)	14.62(18)	14.85(16)
S2900	660	5	1873	1	81.2(5)	73.0(5)	0.63(2)	0.96997(61)	14.98(13)	15.21(11)
S2901	800	5	1873	2	84.5(2)	77.3(5)	0.62(2)	0.96582(84)	15.76(19)	16.00(16)
S2849	650	4	1873	1	93.3(2)	89.6(2)	0.61(1)	0.95447(82)	17.98(21)	18.26(17)
S3255[a]	650	5	1673	1	82.1(4)	73.5(4)	0.61(2)			
S3255[b]					81.3(4)	72.2(4)	0.60(1)			
5K3134[a,e]	360	5	1673	1	82.5(6)	72.6(3)	0.56(2)			
5K3134[b,e]					83.3(7)	74.3(7)	0.58(3)			

[a] Indicates Fo_{80} powder was used as starting materials.
[b] Mixture of Fo_{97} and Fo_{70}, which bulk composition is Fo_{80}, was used as starting material.
[c] $K_D = (X^{Wd}_{Fe}/X^{Wd}_{Mg})/(X^{Rw}_{Fe}/X^{Rw}_{Mg})$.
[d] Pressure was kept larger than pressure just after reached at a desired temperature using addition compression from 65 to 720 ton.
[e] 5 K press, which is the [111] type multi-anvil press was used.

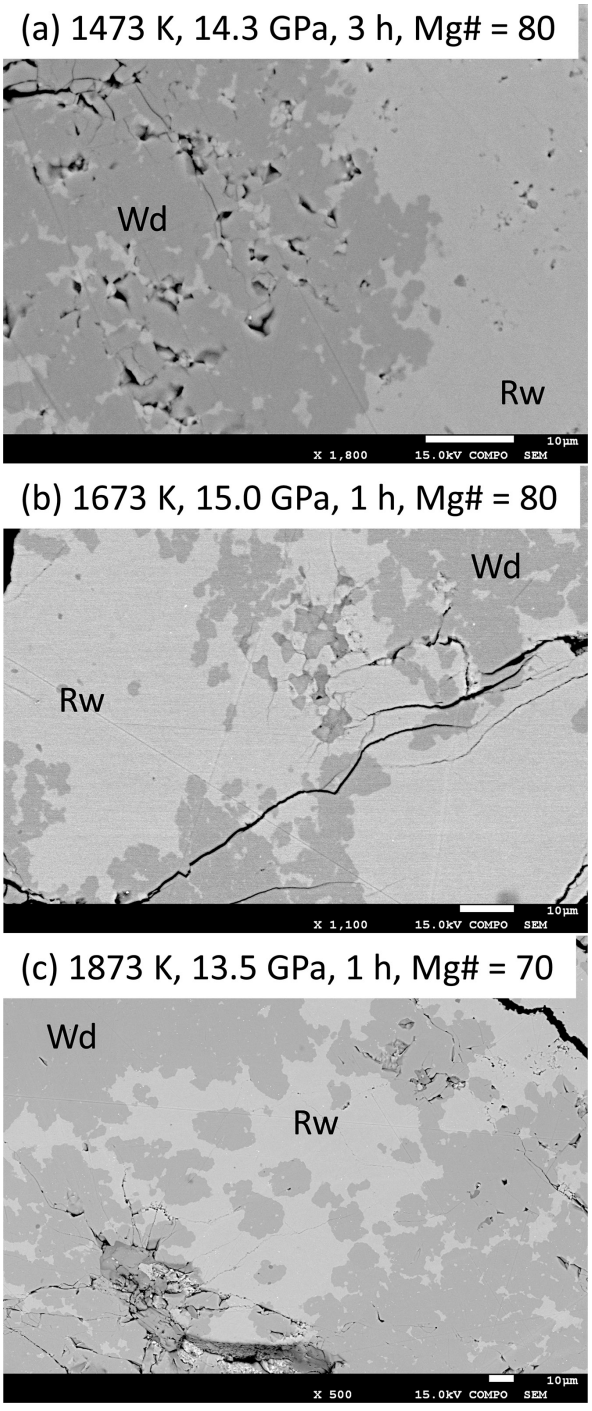

FIGURE 2. Backscattered electron images of recovered samples in (**a**) S2840 (1473 K, 14.3 GPa, 3 h), (**b**) S2823 (1673 K, 15.0 GPa, 1 h), and (**c**) S2838 (1873 K, 13.5 GPa, 1 h). Bright and dark portions denote ringwoodite and wadsleyite, respectively. Wd = wadsleyite; Rw = ringwoodite.

RESULTS AND DISCUSSION

Experimental conditions and results of the in situ X-ray diffraction are summarized in Table 1. High-pressure experiments were conducted at 1473–1873 K and 12.6–18.0 GPa using the MgO scale of Tange et al. (2009). Figure 2 shows typical backscattered electron images of the recovered samples synthesized at 1473–1873 K. There was no heterogeneity in the chemical composition of each phase (wadsleyite and ringwoodite) obtained from each experiment. The partitioning coefficient K_D values of Fe and Mg between wadsleyite and ringwoodite, following $K_D = (X_{Fe}^{Wd}/X_{Mg}^{Wd})/(X_{Fe}^{Rw}/X_{Mg}^{Rw})$, are nearly identical at 1673 K regardless of the composition, starting material type, and run duration (1 to 8 h) including the quench experiments (see Fig. 3 and Table 1). Inoue et al. (2010a, 2010b) also determined the phase relation of olivine composition in dry and wet systems by quench experiments at 1673 K. The K_D determined by Inoue et al. (2010a, 2010b) is consistent with that determined in this study. At 1873 K, chemical equilibrium was achieved faster than at 1673 K. The diffusion coefficients for wadsleyite and ringwoodite at 1473 K are three to four times lower than those at 1673 K based on the activation enthalpies of the Mg-Fe interdiffusion on wadsleyite (143 kJ/mol at x = 0.90) by Kubo et al. (2004). Therefore, the annealing time at 1473 K was set to be greater than three times the shortest annealing time (1 h) at 1673 K. At 1473 K, the samples were also expected to be in chemical equilibrium because of the longer annealing time. Indeed, the K_D values determined in this study at 1473 K are also nearly identical. Katsura and Ito (1989) studied the phase relation of olivine and its high-pressure polymorphs up to 21 GPa at 1873 K and 1473 K using quench experiments. These K_D values in Katsura and Ito (1989) are consistent with those of this study. It can be concluded that all in situ experiments reached chemical equilibrium.

Figure 4 illustrates the phase relations of the polymorphs of olivine in the dry $(Mg,Fe)_2SiO_4$ system at various temperatures with the pressure calculated using the 3BM of MgO by Tange et al. (2009). At each temperature, the binary loop between wadsleyite and ringwoodite was determined using the present

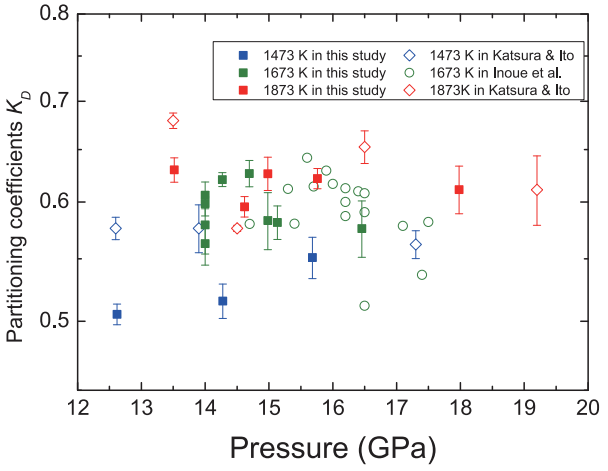

FIGURE 3. Partitioning coefficient K_D values of Fe and Mg between wadsleyite and ringwoodite against pressure under a dry condition and temperatures from 1473 to 1873 K. Solid square, open circle, and open diamond symbols correspond to the present study, Inoue et al. (2010a, 2010b) and Katsura and Ito (1989), respectively. Blue, green, and red color symbols indicate results determined at 1473, 1673, and 1873 K, respectively. (Color online.)

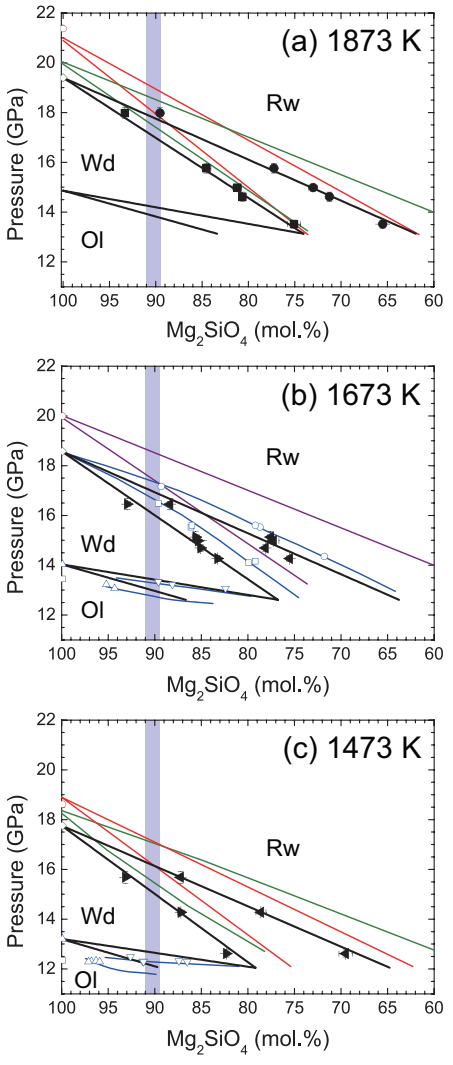

FIGURE 4. Phase relations of olivine composition at (**a**) 1873 K, (**b**) 1673 K, and (**c**) 1473 K. The black triangles are ringwoodite and wadsleyite compositions on the phase boundary loop under dry conditions in this study. Black lines represent the phase boundary loop between olivine, wadsleyite, and ringwoodite based on Katsura et al. (2004) and the present study using the 3BM of Tange et al. (2009). The red, green, and purple lines show the phase boundary loop between wadsleyite and ringwoodite under dry conditions according to Katsura and Ito (1989), Akaogi et al. (1989), and Frost (2003), respectively. Blue circles and squares illustrate the ringwoodite and wadsleyite composition on the phase boundary loop under wet conditions according to Inoue et al. (2010a, 2010b) recalculated using the dry phase boundary data from the present study. Blue triangles and inverse triangles indicate the ringwoodite and wadsleyite composition on the phase boundary loop reported by Inoue et al. (2010a, 2010b) and Chen et al. (2002) recalculated using the dry phase boundary data from Katsura et al. (2004) with the 3BM of Tange et al. (2009). The blue lines represent the phase boundary loop between olivine, wadsleyite, and ringwoodite under wet condition based on Inoue et al. (2010a, 2010b) and Chen et al. (2002). The blue region shows the compositional range of olivine $(Mg_{0.89}Fe_{0.11})_2SiO_4$, wadsleyite $(Mg_{0.90}Fe_{0.10})_2SiO_4$, and ringwoodite $(Mg_{0.905}Fe_{0.095})_2SiO_4$ proposed by Frost (2003). Ol = olivine; Wd = wadsleyite; Rw = ringwoodite. (Color online.)

results of the iron-bearing compositions with Mg-end-members determined by the in situ X-ray diffraction observation of Inoue et al. (2006) at approximately 1673 K, although Suzuki et al. (2000) also determined that the phase boundary between wadsleyite and ringwoodite in Mg_2SiO_4 at low temperatures (873–1273 K). The phase boundary determined by Inoue et al. (2006) was suitable to adopt as the fixed point of the binary loop in this study. As shown in Figure 4, there is a discrepancy between the Mg end-member by Suzuki et al. (2000) and the binary loop in this study because of the large extrapolation of temperature in the Mg end-member while the binary loop in this study is nearly consistent with that of Inoue et al. (2006). Figures 4a and 4c show that the pressures and compositional dependence of the phase boundary loop determined by Katsura and Ito (1989) are inconsistent with those in this study. These differences are probably caused by imprecise estimations of pressure during the quench experiments implemented by Katsura and Ito (1989). Akaogi et al. (1989) and Frost (2003) estimated the phase boundary of olivine polymorphs through thermodynamic calculations, as also shown in Figure 4. The compositional dependence on the binary loop is nearly consistent with the calculations reported by Akaogi et al. (1989) and Frost (2003), although the absolute pressure is different from their results. Thermochemical properties of the Fe_2SiO_4 component in wadsleyite may vary considerably because of the limited compositional range of Fe in this mineral. Thermodynamic calculation (Akaogi et al. 1989; Frost 2003) of the phase boundary loop between wadsleyite and ringwoodite may involve considerable uncertainties, particularly regarding the precise determination of the pressure boundary. Pressure determination by in situ X-ray diffraction can be more reliable in determining the phase boundary.

Figures 4b and 4c also show the pressure of the phase boundary loops of the olivine and its polymorphs under wet conditions. The phase boundary loops under wet conditions in previous studies (Chen et al. 2002; Frost and Dolejš 2007; Inoue et al. 2010a, 2010b) were recalculated using the chemical composition of the olivine and its polymorphs under dry conditions. Chen et al. (2002) and Inoue et al. (2010b) showed no evidence of a pressure difference at the Mg-end-member between dry and wet conditions. However, Frost and Dolejš (2007) argued a pressure drop on the phase boundary of olivine and wadsleyite under wet condition. Chen et al. (2002) and Inoue et al. (2010b) performed experiments using only the Mg-end-member composition in an AuPd capsule to determine the transitional pressure of the Mg-end-member, while Frost and Dolejš (2007) reported experimental results of a Fe-bearing sample used as a pressure indicator in the Al_2O_3 capsule, which is a quite hard material. The discrepancy in the pressure drop between these previous studies might have been caused by a difference in the pressure indicator and/or capsule materials. In the Fe-bearing system, the binary loop between olivine and wadsleyite shifted to a lower pressure under wet condition (Chen et al. 2002), whereas that between wadsleyite and ringwoodite shifted to higher pressure (Inoue et al. 2010a, 2010b). As a result, the stability field of wadsleyite broadened under wet condition. This could have been caused by the higher water solubility of wadsleyite among its polymorphs and water partitioning among its polymorphs under wet condition (e.g., $D_{Wd/Ol} \sim 5$ by Chen et al. 2002; $D_{Wd/Rw} \sim 2$ by Inoue

et al. 2010). In contrast, the pressure difference in the binary loops between dry and wet conditions decreases with increasing temperature from 1473 to 1673 K. In addition, the water solubility of wadsleyite decreases with increasing temperature above 1467 K (Demouchy et al. 2005). The temperature dependence of the binary loops would be influenced by the water solubility of the minerals. Recently, the presence of ferric iron in wadsleyite and ringwoodite has been well known (Frost and McCammon 2009; Mrosko et al. 2015). The stability field of wadsleyite tends to become wider with increasing ferric iron under oxidized conditions. However, to discuss the quantitative effects of ferric iron on the binary loops at each temperature, available data are not sufficient.

Implications for the 520 km seismic discontinuity

Figure 5 shows the phase relations of the olivine composition coexisting with garnet in the pyrolite model under dry and wet conditions assuming 1550–1650 K for the mantle potential temperature. McKenzie and Bickle (1988) estimated the mantle potential temperature below the mid-ocean ridges to be 1550 K or higher from the composition of mid-ocean ridge basalt (MORB). Geochemical study (Herzberg et al. 2007) and another study combining seismology and petrology (Courtier et al. 2007) have also suggested that the potential temperature at the mid-ocean ridges is 1623 ± 50 K. The mantle geotherm would be calculated as an adiabatic temperature gradient except for the surface and bottom regions in which heat flow is controlled by thermal conduction.

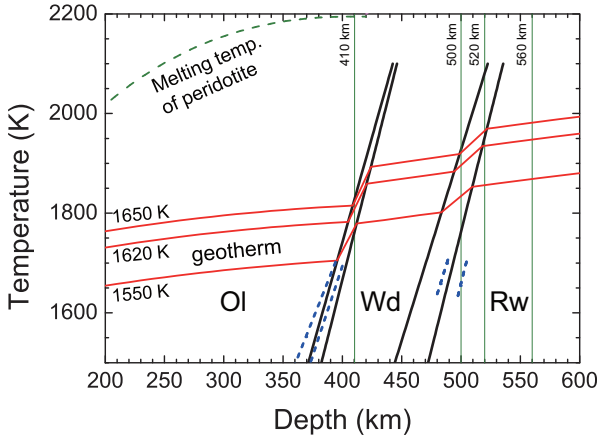

Figure 5. Temperature profile in the normal mantle. The black solid and blue dashed lines represent the phase boundaries of the olivine-wadsleyite-ringwoodite transition under dry and wet conditions, respectively. Compositions of olivine, wadsleyite, and ringwoodite are $(Mg_{0.89}Fe_{0.11})_2SiO_4$, $(Mg_{0.90}Fe_{0.10})_2SiO_4$, and $(Mg_{0.905}Fe_{0.095})_2SiO_4$, respectively, as proposed by Frost (2003). The bold red solid lines represent geotherms in the mantle estimated from the mantle adiabatic and potential temperatures (1550, 1620, and 1650 K) under dry conditions. The green broken line represents the melting temperature curve of the dry fertile peridotite according to Zhang and Herzberg (1994). The green solid lines indicate 410, 500, 520, and 560 km in depth, which corresponds to the seismic discontinuity of Gu et al. (1998) and Deuss and Woodhouse (2001). Ol = olivine; Wd = wadsleyite; Rw = ringwoodite. (Color online.)

The adiabatic temperature gradient (dT/dz) in terms of pressure (or depth) is expressed as follows:

$$(dT/dz) = \alpha g T/C_P \quad (1)$$

where α is the thermal expansion coefficient, g is the gravity constant, T is the temperature, and C_P is the specific heat capacity at a constant pressure. The C_P of each mineral has been summarized by Akaogi et al. (1989). In addition, the adiabatic temperature profile in the mantle changes during phase transitions because of the latent heat. The change in temperature caused by the latent heat is described as follows:

$$\Delta T_{latent} = T\Delta V(dP/dT)/C_P \quad (2)$$

where ΔT_{latent} is the change in the temperature caused by latent heat, (dP/dT) is the Clapeyron slope of the phase transition, and ΔV is the volume change resulting from the phase transition. Suzuki et al. (2000) and Inoue et al. (2006) reported a Clapeyron slope of 6.91 and 4.11 MPa/K for the wadsleyite-ringwoodite phase transition, respectively. The ΔV was calculated by the equation of the state of wadsleyite and ringwoodite by Liu et al. (2009) and Nishihara et al. (2004), respectively. Using these values, the change in temperature resulting from latent heat was calculated to be 43–26 K. To calculate the mantle geotherm, 26 K was used because the results of this study agree well with those of Inoue et al. (2006). We used the latent heat (60 K) for the olivine-wadsleyite phase transition by Katsura et al. (2004).

The seismic reflection plane formed by the olivine-wadsleyite phase boundary corresponds to the plane where the ratio of olivine to wadsleyite is 1:2 (Stixrude 1997). From the adiabatic temperature gradient of 1550 to 1650 K for the potential temperature proposed by previous studies, the depth of the reflection plane under dry condition was estimated to be 407–419 km at a temperature of 1754–1867 K as shown in Figure 5. The 410 km seismic discontinuity is globally observed as a depth ranging between 411 km and 418 km (Gu et al. 1998; Flanagan and Shearer 1998), corresponding to the phase boundary between olivine and wadsleyite under dry condition. In the presence of H_2O, the phase boundary shifts to a shallower depth with decreasing temperature. However, within the expected temperature range (1754–1867 K) at 410 km depth, the effect of water on the phase boundary could be very small because the water solubility of wadsleyite decreases with increasing temperature (Demouchy et al. 2005). Even under wet conditions, the depth of the phase boundary at a 1550–1650 K potential temperature is still consistent with the 410 km discontinuity.

The depth of the seismic reflection plane caused by the phase transition between wadsleyite and ringwoodite under dry condition was calculated to be 500–514 km depth at a temperature of 1850–1950 K. Compared to the olivine-wadsleyite binary loop, the binary loop between wadsleyite and ringwoodite is much thicker, and thus it is more difficult to detect it as a seismic discontinuity. The effective width of the binary phase transition was estimated to be 20–22 km with $K_D = 0.63$ at 1873 K based on Stixrude (1997). This effective width, which is three times larger than that of the olivine-wadsleyite phase boundary by Katsura et al. (2004), can reflect a seismic P wave of approximately 0.25 Hz (Stixrude 1997). The wadsleyite-ringwoodite binary loop

is much broader than the olivine-wadsleyite phase boundary for seismic observations. Under wet condition at 1673 K, the depth of the phase boundary is greater (~13 km) than that under dry condition while the effect of water on the olivine-wadsleyite binary loop decreases with increasing temperature. The pressure interval of the wadsleyite-ringwoodite binary loop can decrease with increasing temperature. Mrosko et al. (2015) also suggested that the depth of the wadsleyite–ringwoodite phase transition deepened (~13 km corresponding to ~0.5 GPa) with oxidation conditions from the Fe-FeO buffer to Re-ReO_2 buffer at 1473 K under wet condition. There is a possibility that the transitional pressure between wadsleyite and ringwoodite increases under an oxidation state assuming a small temperature effect on oxygen fugacity. The 520 km seismic discontinuity (Gossler and Kind 1996; Deuss and Woodhouse 2001) has been confirmed in some regions (e.g., India and central Asia) but has been found to be absent in other regions (e.g., the northeastern Pacific Ocean and the northern Atlantic Ocean). In addition, analysis using a longer period shear wave (Deuss and Woodhouse 2001; Tian et al. 2016), which allows for detection of broader phase transitions, suggests two seismic discontinuities at 500 and/or 560 km instead of one 520 km seismic discontinuity (e.g., under North Africa, North America, and Indonesia). The 500 km seismic discontinuity can be explained by the shallower wadsleyite-ringwoodite phase transition under dry and Mo-MoO_2 buffer conditions. On the other hand, chemical heterogeneity including water and oxygen fugacity of the mantle transitional zone would remain unchanged over the geological timescale, even under conditions of fastest hydrogen self-diffusion (Sun et al. 2015, 2018). When the mantle transition zone has heterogeneous water content and oxygen fugacity, the depth of the wadsleyite-ringwoodite phase boundary could be deeper than that under dry and reducing conditions (Mo-MoO_2 buffer). Therefore, the seismic discontinuity of the depth from 500 to 520 km can be explained by the wadsleyite-ringwoodite phase boundary with water and oxygen fugacity heterogeneities. At approximately 560 km depth, there are a few minor candidates that may cause the observed seismic discontinuity, e.g., the exsolution of Ca-perovskite from garnet (Ita and Stixrude 1992; Saikia et al. 2008), which is among the major constitute minerals in MORB (Saikia et al. 2008).

Funding

This work was supported by the Grant-in-Aid for JSPS Fellows (15J09669) and Grant-in-Aid for Scientific Research (B) (18H01314) to N.T. The in situ X-ray diffraction experiments implemented to precisely determine pressure were conducted on the BL04B1 at SPring-8 under the approval of the JASRI (Proposal Nos. 2012B1437, 2013A1475, 2013B1434, 2014A1431, 2014B1400, 2015A1600, 2015B1504, 2017A1525, 2017B1329, and 2018A1457).

Acknowledgments

We thank Toshihiro Suzuki for many helpful comments. We are grateful to Anwar Mohiuddin for reading the manuscript and providing constructive comments. We appreciate HACTO group member for their help in obtaining diffraction data.

References cited

Akaogi, M., Ito, E., and Navrotsky, A. (1989) Olivine-modified spinel-spinel transitions in the system Mg_2SiO_4-Fe_2SiO_4 calorimetric measurements, thermochemical calculation, and geophysical application. Journal of Geophysical Research, 94, 15671–15685.

Chen, J., Inoue, T., Yurimoto, H., and Weidner, D.J. (2002) Effect of water on olivine-wadsleyite phase boundary in the $(Mg,Fe)_2SiO_4$ system. Geophysical Research Letters, 29, doi:10.1029/2001GL014429.

Courtier, A.M., Jackson, M.G., Lawrence, J.F., Wang, Z., Aelous Lee, C., Halama, R., Warren, J.M., Workman, R., Xu, W., Hirschmann, M.M., and others. (2007) Correlation of seismic and petrologic thermometers suggests deep thermal anomalies beneath hotspots. Earth and Planetary Science Letters, 264, 308–316.

Demouchy, S., Deloule, E., Frost, D.J., and Keppler, H. (2005) Pressure and temperature-dependence of water solubility in Fe-free wadsleyite. American Mineralogist, 90, 1084–1091.

Deuss, A., and Woodhouse. (2001) Seismic observations of splitting of the mid-transition zone discontinuity in Earth's mantle. Science, 294, 354–357.

Dziewonski, A.D., and Anderson, D.L. (1981) Preliminary Reference Earth Model. Physics of the Earth and Planetary Interiors, 25, 297–356.

Flanagan, M.P., and Shearer, P.M. (1998) Global mapping of topography on transition zone velocity discontinuities by stacking SS precursors. Journal of Geophysical Research, 103, 2673–2692.

Frost, D.J. (2003) The structure and sharpness of $(Mg,Fe)_2SiO_4$ phase transformations in the transition zone. Earth and Planetary Science Letters, 216, 313–328.

Frost, D.J., and Dolejš, D. (2007) Experimental determination of the effect of H_2O on the 410-km seismic discontinuity. Earth and Planetary Science Letters, 256, 182–195.

Frost, D.J., and McCammon, C.A. (2009) The effect of oxygen fugacity on the olivine to wadsleyite transformation: Implications for remote sensing of mantle redox state at the 410 km seismic discontinuity. American Mineralogist, 94, 872–882.

Gossler, J., and Kind, R. (1996) Seismic evidence for very deep roots of continents. Earth and Planetary Science Letters, 138, 1–13.

Gu, Y., Dziewonski, A.M., and Agee, C.B. (1998) Global de-correlation of the topography of transition zone discontinuities. Earth and Planetary Science Letters, 157, 57–67.

Helffrich, G. (2000) Topography of the transition zone seismic discontinuity. Reviews of Geophysics, 38, 141–158.

Herzberg, C., Asimow, P.D., Arndt, N., Niu, Y., Lesher, C.M., Fitton, J.G., Cheadle, M.J., and Saunders, A.D. (2007) Temperatures in ambient mantle and plumes: Constraints from basalts, picrites, and komatiites. Geochemistry, Geophysics, Geosystems, 8, 2, doi:10.1029/2006GC001390.

Inoue, T., Irifue, T., Higo, T., Sanehira, T., Sueda, Y., Yamada, A., Shinmei, T., Yamazaki, D., Ando, J., Funakoshi, K., and Utsumi, W. (2006) The phase boundary between wadsleyite and ringwoodite in Mg_2SiO_4 determined by in situ X-ray diffraction. Physics and Chemistry of Minerals, 33, 106–114.

Inoue, T., Wada, T., Sasaki, R., and Yurimoto, H. (2010a) Water partitioning in the Earth's mantle. Physics of the Earth and Planetary Interiors, 183, 245–251.

Inoue, T., Ueda, T., Yanimoto, Y., Yamada, A., and Irifune, T. (2010b) The effect of water on the high-pressure phase boundaries in the system Mg_2SiO_4-Fe_2SiO_4. Journal of Physics: Conference Series, 2015, 012101.

Ita, J., and Stixrude, L. (1992) Petrology, elasticity, and composition of the mantle transition zone. Journal of Geophysical Research, 97, B, 5, 6849–6866.

Katsura, T., and Ito, E. (1989) The system Mg_2SiO_4-Fe_2SiO_4 at high pressures and temperatures: Precise determination of stabilities of olivine, modified spinel, and spinel. Journal of Geophysical Research, 94, 15,663–15,670.

Katsura, T., Yamada, H., Nishikawa, O., Song, M., Kubo, A., Shinmei. T., Yokoshi, S., Aizawa, Y., Yoshino, T., Walter, M.J., and Ito, E. (2004) Olivine-wadsleyite transition in the system $(Mg,Fe)_2SiO_4$. Journal of Geophysical Research, 109, doi:10.1029/2003JB002438.

Kennett, B.L.N., and Engdahl, E.R. (1991) Travel times for global earthquake location and phase identification. Geophysical Journal International, 105, 429–465.

Kubo, T., Shimojuku, and, A., Ohtani, E. (2004) Mg-Fe interdiffusion rates in wadsleyite and the diffusivity jump at the 410-km discontinuity. Physics and Chemistry of Minerals, 31, 456–464.

Liu, W., Kung, J., Li, B., Nishiyama, N., Wang, Y. (2009) Elasticity of $(Mg_{0.87}Fe_{0.13})_2SiO_4$ wadsleyite to 12 GPa and 1073 K. Physics of the Earth and Planetary Interiors, 174, 98–104.

McKenzie, D., and Bickle, M.J. (1988) The volume and composition of melt generated by extension of the lithosphere. Journal of Petrology, 29, 623–679.

Morishima, E., Kato, Suto, M., Ohtani, E., Urakawa, S., Utsumi, W., Shimomura, O., and Kikekgawa, T. (1994) The phase boundary between α- and β-Mg_2SiO_4 determined by in situ X-ray observation. Science, 265, 1202–1203.

Mrosko, M., Koch-Müller, M., McCammon, C., Rhede, D., Smyth, J.R., and Wirth, R. (2015) Water, iron, redox environment: effects on the wadsleyite-ringwoodite phase transition. Contributions to Mineralogy and Petrology, 170, 9, DOI: 10.1007/s00410-015-1163-2.

Nishihara, Y., Takahashi, E., Matsukage, K.N., Iguchi, T., Nakayama, K., and Funakoshi, K. (2004) Thermal equation of state of $(Mg_{0.91}Fe_{0.09})_2SiO_4$ ringwoodite. Physics of the Earth and Planetary Interiors, 143-144, 33–46.

Nishiyama, N., Irifune, T., Inoue, T., Ando, J.I., and Funakoshi, K.I. (2004) Precise determination of phase relations in pyrolite across the 660 km seismic discontinuity by in situ X-ray diffraction and quench experiments. Physics of the Earth and Planetary Interiors, 143, 185–199.

Saikia, A., Frost, D.J., and Rubie, D.C. (2008) Splitting of the 520-kilometer Seismic Discontinuity and Chemical Heterogeneity in the Mantle. Science, 319, 1515–1518.

Shearer, P.M. (1990) Seismic imaging of upper-mantle structure with new evidence

for a 520-km discontinuity. Nature, 344, 121–126.
——— (1991) Constrains on upper mantle discontinuity from observations of long-period reflected and converted phases. Journal of Geophysical Research, 96, 18,147–18,182.
Speziale, S., Zha, C., Duffy, T.S., Hemley, R.J., and Mao, H. (2001) Quasi-hydrostatic compression of magnesium oxide to 52 GPa: Implications for the pressure-volume-temperature equation of state. Journal of Geophysical Research, 106, 515–528.
Stixrude, L. (1997) Structure and sharpness of phase transitions and mantle discontinuities. Journal of Geophysical Research, 102, B, 7, 14,835–14,852.
Sun, W., Yoshino, T., Sakamoto, N., and Yurimoto, H. (2015) Hydrogen self-diffusivity in single crystal ringwoodite: Implications for water content and distribution in the mantle transition zone. Geophysical Research Letters, DOI: 10.1002/2015GL064486.
——— (2018) Supercritical fluid in the mantle transition zone deduced from H/D interdiffusion of wadsleyite. Earth and Planetary Science Letters, 484, 309–317.
Suzuki A., Othtani, E., Morishima, H., Kubo, T., Kanbe, Y., and Kondo, T. (2000) In situ determination of the phase boundary between wadsleyite and ringwoodite in Mg_2SiO_4. Geophysical Research Letters, 27, 803–806.
Tange, Y., Nishihara, Y., and Tsuchiya, T. (2009) Unified analyses for *P-V-T* equation of state of MgO: A solution for pressure-scale problems in high *P-T* experiments. Journal of Geophysical Research, 114, B03208, doi:10.1029/2008JB005813.
Tian, Y., Zhu, H., Zhao, D., Liu, C., Feng, X., Liu, T., and Ma, J. (2016) Mantle transition zone structure beneath the Changbai volcano: Insight into deep slab dehydration and hot upwelling near the 410 km discontinuity. Journal of Geophysical Research, 121, 5794–5808, doi:10.1002/2016JB012959.
Utsumi, W., Funakoshi, K., Urakawa, S., Yamakata, M., Tsuji, K., Konishi, H., and Shimomura, O. (1998) SPring-8 beamlines for high pressure science with multi-anvil apparatus. The Review of High Pressure Science and Technology, 7, 1484–1486.
Zhang, J., and Herzberg, C. (1994) Melting experiments on anhydrous peridotite KLB-1 from 5.0 to 22.5 GPa. Journal of Geophysical Research, 99, 17,729–17,742.

Manuscript received September 24, 2018
Manuscript accepted January 15, 2019
Manuscript handled by Ryosuke Sinmyo